文章编号：1001-9014(2021)04-0490-06

DOI:10. 11972/j. issn. 1001-9014. 2021. 04. 008

The temperature-dependent phase transition in $La_{0.7}Ca_{0.3}MnO_3$ film probed with terahertz transient spectroscopy

LI Gao-Fang[1,3], XU Yan-Xia[1], LIU Xian-Kuan[2], MA Guo-Hong[2*], GAO Yan-Qing[3], CUI Hao-Yang[1], HUANG Zhi-Ming[3*], CHU Jun-Hao[3]

(1. School of Electronic & Information Engineering, Shanghai University of Electric Power, Shanghai 200082, China;
2. Department of Physics, Shanghai University, Shanghai 200444, China;
3. State Key Laboratory of Infrared Physics, Shanghai Institute of Technical Physics, Chinese Academy of Sciences, Shanghai 200083, China)

Abstract: The thermodynamics of $La_{0.7}Ca_{0.3}MnO_3$ film by terahertz transient spectroscopy were presented. The temperature of metal-insulator phase transition of $La_{0.7}Ca_{0.3}MnO_3$ film is observed to occur around 260 K, which is almost the same as that of the ferromagnetic-paramagnetic phase transition. It indicates that the conductivity of the $La_{0.7}Ca_{0.3}MnO_3$ film is closely related to the order of magnetic moments in the film. We find the conductivity of the $La_{0.7}Ca_{0.3}MnO_3$ film can be reproduced with Drude model at low temperature range from 40 K to 200 K, and Drude-Lorentz model at high temperature region from 210 K to 290 K.

Key words: metal-insulator phase transition, ferromagnetic-paramagnetic phase transition, terahertz conductivity, $La_{0.7}Ca_{0.3}MnO_3$ film

太赫兹瞬态光谱研究$La_{0.7}Ca_{0.3}MnO_3$薄膜的温度相关相变

李高芳[1,3], 许艳霞[1], 刘现款[2], 马国宏[2*], 高艳卿[3], 崔昊杨[1], 黄志明[3*], 褚君浩[3]

(1. 上海电力大学 电子与信息工程学院, 上海 200082;
2. 上海大学 物理系, 上海 200444;
3. 中国科学院上海技术物理研究所 红外物理国家重点实验室, 上海 200083)

摘要: 利用太赫兹瞬态光谱研究了$La_{0.7}Ca_{0.3}MnO_3$薄膜的热力学性质。$La_{0.7}Ca_{0.3}MnO_3$薄膜的金属-绝缘体相变温度在260 K左右, 与铁磁-顺磁相变温度几乎相同。结果表明, $La_{0.7}Ca_{0.3}MnO_3$薄膜的电导率与薄膜中磁矩取向密切相关。研究发现在40~200 K的低温范围内, $La_{0.7}Ca_{0.3}MnO_3$薄膜的电导率可以用Drude模型拟合, 在210~290 K的高温范围内可以用Drude-Lorentz模型拟合。

关 键 词: 金属-绝缘体相变; 铁磁-顺磁相变; 太赫兹电导率; $La_{0.7}Ca_{0.3}MnO_3$薄膜

中图分类号: O433.1　　**文献标识码**: A

Introduction

The trivalent rare earth element doped perovskite oxides $La_{1-x}Ca_xMnO_3$ film exhibits rich electrical and magnetic properties. For example, in $La_{0.7}Ca_{0.3}MnO_3$ membranes, the balance between metallic and insulating phases can be tuned by the lattice, and extending the range of lattice control would enhance the ability to access other phases[1-2]. A colossal magnetoresistance (CMR) phenomenon was reported in a perovskite-like $La_{0.67}Ca_{0.33}MnO_3$ thin oxide films on $LaAlO_3$ (LAO) substrates[3-6]. It is well-known that the CMR effect appears around the metal-insulator transition temperature (T_{MI}), and lots of works were done on the metal-insulator (MI) phase transition based on $La_{1-x}Ca_xMnO_3$ film[7-10]. Below the Curie temperature (T_C), the thin film is ferromagnet-

Received date: 2020-09-29, **revised date**: 2021-04-21　　**收稿日期**: 2020-09-29, **修回日期**: 2021-04-21

Foundation items: Supported by National Natural Science Foundation of China (11674213, 61735010, 11647023, 61625505), Natural Science Foundation of Shanghai (17ZR1411500)

Biography: LI Gao-Fang (1983-), female, Xuchang, China. Ph. D. Research area involves terahertz spectroscopy. E-mail: ligaofang@shiep. edu. cn

*Corresponding author: E-mail: phymagh@t. shu. edu. cn, zmhuang@mail. sitp. ac. cn

ic (FM) phase, and shows a higher conductivity. The film is transformed into paramagnetic (PM) phase with a good insulator above T_C[11-12]. The FM to PM phase transition was attributed to the spin order change in 3d orbit electrons of Mn ions[13]. In $La_{1-x}Ca_xMnO_3$ film, the double exchange interaction between Mn^{3+}-O-Mn^{+4} predicts that ferromagnetic corresponds to metal phase, and paramagnetic corresponds to insulator phase[14-16]. By monitoring the doping proportion of rare element, both T_C and T_{MI} of $La_{1-x}Ca_xMnO_3$ film can be tuned accordingly[17-22]. In addition, the substrate strain also has strong influence on the magnetic transport and the metal-insulator phase transition temperature of the film[23-30].

It was reported that the $La_{0.7}Ca_{0.3}MnO_3$ (LCMO) film showed Drude conductivity when the temperature was below around 0.7 T_C, and the film conductivity was far deviated from the Drude model during the temperature range from 0.7 T_C to T_C[31]. Some literatures reported that the T_{MI} temperature of LCMO epitaxial films was different from the T_C[25]. But T_{MI} was usually measured by contacted electrical measurement, and the contact resistance between electrodes and film had significant influence on the measured value of T_{MI}. It is still controversial whether the T_{MI} and T_C temperature falls the same temperature point or not. Terahertz spectroscopy is contact-free, invasive, and extremely sensitive method to study the metal to insulator phase transition compared to the traditional method. With the advanced THz spectroscopy, the dynamical phase transition from ferromagnetic metal phase to paramagnetic insulator phase can be clarified[31-32], specifically, near the T_C and T_{MI} temperatures, the competitive and coexistence mechanism behind the phase transition can be clarified.

In this paper, the thermodynamics in LCMO film between ferromagnetic metal phase and paramagnetic insulator phase are investigated by the low temperature THz time-domain spectroscopy. The Curie temperature T_C is measured to be the same as the metal-insulator transition temperature T_{MI}. The conductivity of the film can be well reproduced with Drude model from 40 K to 200 K, while its conductivity follows the Drude-Lorentz model in high temperature range from 210 K to 290 K. The experimental results are instrumental to comprehend the electromagnetic and photoelectric properties related to phase transition, and have important application in thermoelectric device, contactless reluctance switch and so on.

1 Samples preparation and experimental results

The LCMO film with thickness of 200 nm (measured with a step profiler) was fabricated on a 0.5-mm, (100)-oriented $LaAlO_3$ single crystal substrate by pulse laser deposition method. The detail process of the film fabrication has been described elsewhere[24]. The temperature dependent conductivity of the LCMO film in THz frequency was characterized with a THz time domain spectroscopy in transmission configuration. The output of a mode-locked Ti: sapphire laser, with pulse duration of 100 fs, centered wavelength of 800 nm, and repetition rate of 80 MHz (Mai Tai HP-1020, Spectra-Physics), was used to generate and detect the THz transient. The THz emitter and detector are a pair of low-temperature-grown GaAs photoconductive antennas. The polarization of the THz radiation is vertical, which is perpendicular to the photoconductive antennas. The effective bandwidth of the THz spectrum is from 0.2 to 2.5 THz. The diameter of THz beam is around 3 mm at the sample position. The sample was placed in a cold finger cryostat with two THz-transparent windows, for which the temperature was tunable in the range of 40 to 300 K with best resolution of 1 K. The characterization of the LCMO film magnetization as a function of temperature was performed on a physical property measurement system (Quantum Design, PPMS-9) under vacuum condition in the temperature range from 10 K to 300 K with temperature stability better than ±0.02%. The temperature dependent magnetization measurement (M-T curve) was carried out separately from THz transmission measurement.

Figure 1(a) shows the transmitted THz electric field through the LCMO film on a 0.5 mm-LAO substrate with three selected temperatures of 100 K, 200 K, and 300 K. Apart from the main pulses localized around~19 ps, it is seen that week signals appear around 36 ps, which correspond to the second-order reflection (or say, echo pulse) of the main pulse at each temperature. With decreasing temperature from 300 K to 40 K, the amplitude of main pulse is seen to decrease, which suggests the increase of the sample conductivity. Moreover, the echo pulse of THz electric field shows in-phase with the main pulse at high temperature (for instance, 300 K), and shows a π-phase shift at low temperature (100 K). The echo pulse disappears completely around ~200 K. In order to exclude the contribution from LAO substrate, Fig. 1(b) shows the transmitted time-domain THz electric field of a 0.5-mm LAO single crystal, it is seen that both main pulse and echo pulse show almost no observable change with temperature. Thus the temperature dependent THz echo pulse signals come from the temperature dependent conductivity of the LCMO thin film[33].

Firstly, we focus on the LCMO film conductivity change with temperature. Figure 2(a) presents the transmitted THz amplitude of the sample as a function of temperature at several frequencies; an obvious turning point occurring at 260 K is seen for all selected frequencies: the transmitted THz amplitude increases near linearly with temperature in the temperature range from 40 K to 260 K, reaches a maximum value at about 260 K, and it is almost unchanged in the temperature range from 260 K to 280 K. Figure 2(b) shows magnetization of the LCMO thin film as a function of temperature for comparison. The magnetization of the film is seen to decrease rapidly with temperature in the temperature range from 260 K to 280 K. Figure 2(d) shows the dM/dT (derivation of magnetization with temperature) as a function of temperature. The minimum value of dM/dT is found to be the same with the turning point (~260 K) in the temperature dependent THz transmission. The real part of complex film conductivity in Fig. 2(c) is obtained from the THz

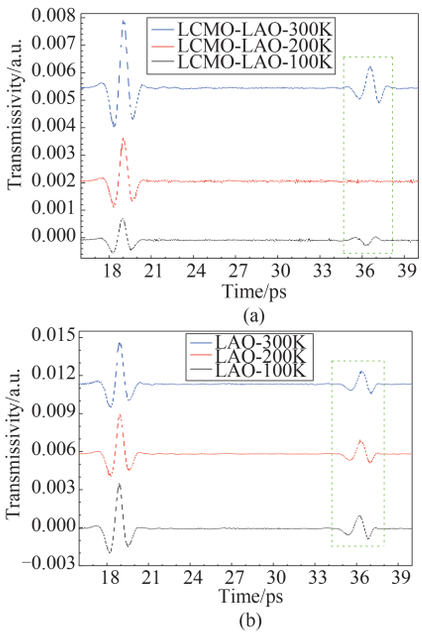

Fig. 1 (a) THz time domain transmission signals of LCMO film on a 0.5-mm LAO substrate at 100 K, 200 K, and 300 K, respectively, (b) THz transmission signals of 0.5-mm LAO substrate at 100 K, 200 K, and 300K, respectively. The green rectangles highlight the echo pulse occurring at the interface of LCMO/LAO (a) and vacuum/LAO (b)

图1 (a) 温度分别为100 K、200 K和300 K时, 0.5-mm LAO衬底上长有LCMO薄膜的THz时域透射信号, (b) 温度分别为100 K、200 K和300 K时, 0.5-mm LAO衬底的THz透射信号。绿色矩形突出显示了LCMO/LAO (a) 和vacuum/LAO (b) 界面处的回波脉冲

amplitude transmission shown in Fig. 2(a) with Eq. 1[34],

$$\sigma_r = \left(\frac{\cos\varphi}{A} - 1\right)\frac{1 + n_{sub}}{Z_0 d} \quad , \quad (1)$$

here, φ and A represent the THz phase and amplitude difference between LCMO/LAO and LAO substrate, respectively. n_{sub}, d, and Z_0 are the refractive index of the LAO substrate, the thickness of the LCMO film, and the free space impedance (with Z_0=377 Ω). With the thickness of the LCMO film d=200 nm, we give the real part of complex conductivity of the LCMO film, σ_r. It is also noted that the real part of complex conductivity changes as a function of temperature shows a turning point around 260 K in Fig. 2(c). The real part of film conductivity decreases near linearly with temperature in the temperature range from 40 K to 260 K, and reaches a minimum value at 260 K. By increasing temperature further, the THz conductivity remains a constant in the temperature range from 260 K to 280 K. The turning temperature of THz conductivity occurring at about 260 K represents the metal-insulator phase transition temperature. In contrast, by looking at the temperature dependent magnetization shown in Figs. 2(b) and 2(d), the magnetic phase transition temperature is also around 260 K. Based on Fig. 2, we can conclude that the LCMO is magnetically ordered metallic phase when temperature is lower than 260 K. When the temperature is higher than 260 K, the LCMO film lies at paramagnetic insulating phase. The metal to insulator phase transition occurs at the same temperature for the FM to PM phase transition.

Then, let's focus on the THz pulse second order reflection occurring at the LCMO/LAO film interface. Figure 3(a) shows the THz echo pulse occurring at the interface of LCMO thin film at three selected temperatures of 198 K, 204 K, and 210 K, respectively. The echo pulse disappears completely at ~204 K, when temperature is higher than 204 K, the echo pulse show in-phase with the input main THz pulse, and when temperature is lower than 204 K, the echo pulse shows a π-phase shift with respect to the main pulse. Figure 3(b) schematically shows the THz pulse reflection occurring at the interfaces of the substrate LAO with different temperature. When temperature is below 200 K, LCMO shows a higher conductivity, and the refractive index difference between substrate and vacuum is smaller than $Z_0\sigma_r$, i. e., n_{sub}-1< $Z_0\sigma_r$, THz pulse experiences reflection at the LCMO/LAO interface and reflected THz pulse has a π-phase shift with the incident pulse. As the temperature is above 210 K, we have n_{sub}-1>$Z_0\sigma_r$, THz pulse reflection occurs at the interface between LCMO film and vacuum, therefore the reflected THz pulse is in-phase with the incident pulse. Among 200 K and 210 K, n_{sub}-1≈$Z_0\sigma_r$, in which case impedance matching condition between vacuum and LAO substrate is met, thus the incident THz pulse does not experience reflection at the interface, as a result, the THz echo pulse disappears in this temperature.

2 Results and discussions

To understand the carriers' thermodynamics of the LCMO film in THz region, we employ Drude-Lorentz model as shown in Eq. 2[35] to reproduce the conductivity at all investigated temperatures.

$$\sigma(\omega) = \frac{Ne^2}{m^*}\frac{\tau}{(1 - (i\tau(\omega - \omega_0^2/\omega)))} \quad , \quad (2)$$

here N, e, m^* and τ are the carrier density, carrier charge, effective mass of carrier and scattering time, respectively. ω_0 denotes the resonant frequency of the system. When ω_0=0, the Drude-Lorentz model is reduced to Drude model that is usually used to describe the free electron response, such as metal-like materials. Below the

Curie temperature, T_C, LCMO film behaves a metallic phase and the Drude model is expected to fit the film conductivity. However, it is found that Drude model can only reproduce the film conductivity at low temperature below 200 K (~0.77 T_C). The solid lines in Figs. 4(a) and (b) show the fitted curves at 40 K and 200 K, respectively. Both real and imaginary parts can be reproduced with Drude model when temperature is lower than 200 K. As temperature is above 200 K and below 260 K (T_C), although the film is still in metallic magnetic phase, it is seen that the imaginary part of the conductivity exhibits negative value as given in Fig. 4(c), which indicates that the Lorentz parameter is not equal to zero (i. e., $\omega_0 \neq 0$) at this temperature region. The solid lines in Fig. 4(c-d) are fitting lines with Drude-Lorentz model, and the fitting parameter, ω_0, as a function of temperature is given in Fig. 5(c). Thus, among the tempera-

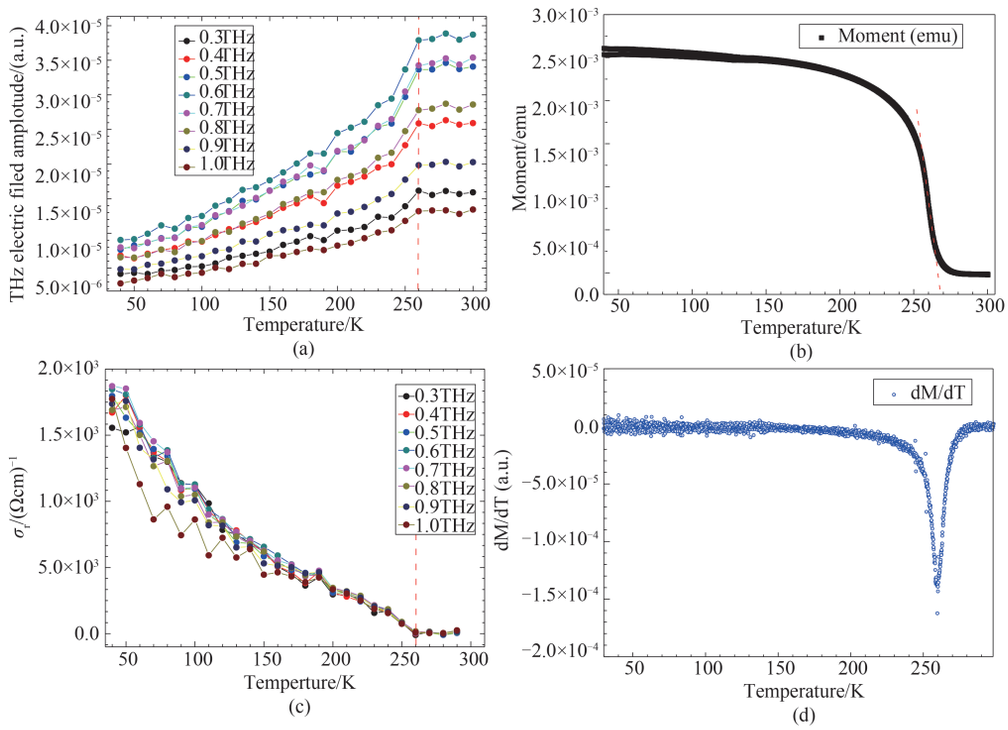

Fig. 2 (a) THz electric field amplitude transmission of LCMO film as a function of temperature at several frequencies, (b) Temperature dependent magnetization of LCMO film, as measured in field cooling condition with the applied magnetic field of 500 Oe, (c) Conductivity (real part) of LCMO film with temperature at several frequencies, (d) dM/dT as a function of temperature for the LCMO film
图 2 (a) LCMO 薄膜在不同频率下 THz 电场振幅随温度的变化,(b) 在外加磁场为 500 Oe 时, LCMO 薄膜磁化强度随温度的变化, (c) 不同频率下 LCMO 薄膜的电导率(实部)随温度的变化,(d) LCMO 薄膜 dM/dT 随温度的变化

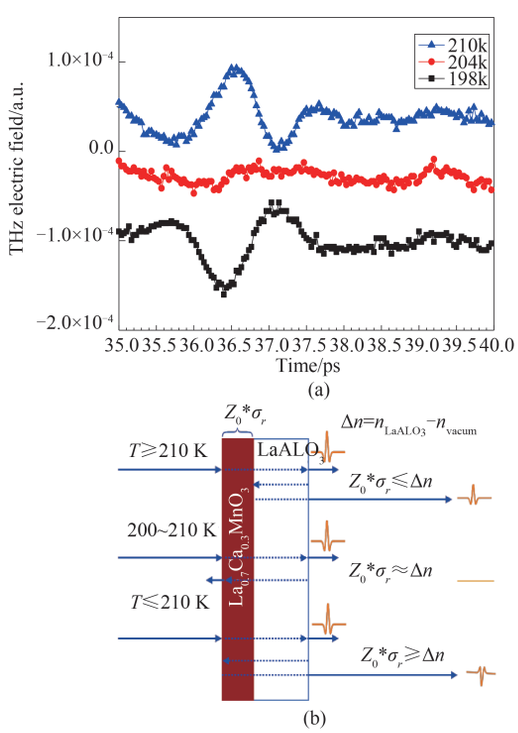

Fig. 3 (a) The THz echo pulses in time domain at 198 K, 204 K, 210 K, (b) The diagram of terahertz pulses come across sample ($La_{0.7}Ca_{0.3}MnO_3$ /$LaAlO_3$) at different temperature
图 3 (a) 温度为 198 K、204 K、210 K 时 La0.7Ca0.3MnO3/LaAlO3 的时域 THz 回波脉冲,(b) 不同温度下太赫兹脉冲通过样品 (La0.7Ca0.3MnO3 /LaAlO3)的示意图

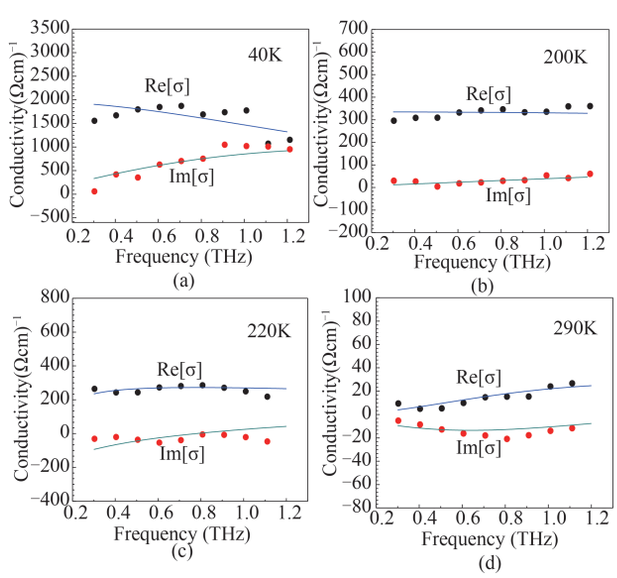

Fig. 4 The complex conductivity of LCMO film at four selected temperatures (a)40 K, (b)200 K, (c)220 K, and (d)290 K
Note: The black and red dots are denoted for real and imaginary part of conductivity, respectively. In (a) and (b), the solid lines are fitting curves with Drude model. In (c) and (d), the solid lines are fitting curves with Drude-Lorentz model. The fitting parameters are presented in Fig. 5
图 4 (a)40 K、(b)200 K、(c)220 K,(d)290 K
注:黑点和红点分别表示复电导率的实部和虚部;在 (a)和 (b)中, 实线是 Drude 模型的拟合曲线;(c) 和 (d) 中, 实线是 Drude-Lorentz 模型的拟合曲线。拟合参数如图 5 所示

ture interval between 0.77 T_C (200 K) and T_C (260 K), the competition between ferromagnetic metal and paramagnetic insulator dominates the terahertz conductivity.

According to Drude-Lorentz model in Eq. 2, some temperature dependent fitting parameters are plotted in Fig. 5. Figure 5(a) shows the temperature dependent plasma frequency (ω_p, $\omega_P = \left(Ne^2/m^*\varepsilon_\infty\varepsilon_0\right)^{1/2}$) of LCMO film between 40 K and 290 K. As the plasma frequency is proportional to the square root of carrier density, it is seen from Fig. 5(a) that the carrier density in LCMO film decreases with temperature from 40 K to 180 K. By further increasing the temperature, the carrier density is seen to increase rapidly from 180 K to 200 K, and reach a maximum at 200 K. As the temperature is higher than 200 K, the carrier density of the film decreases gradually with increasing temperature to 290 K. The fitting scattering time (τ) presented in Fig. 5(b) demonstrates a non-monotonous change with temperature in the temperature range from 40 K to 200 K: the magnitude of τ is seen to increase from 40 K to 90 K, then decrease from 90 K to 200 K. It is noted from Fig. 2(b) that the magnetization of LCMO film remains almost a constant from 40 K to 90 K, but decreases slowly from 90 K to 200 K, and decreases sharply in the temperature range from 200 K to 260 K. Because the magnetization is strongly correlated with spin order of Mn^{3+} and Mn^{4+} ions, non-temperature dependence of magnetization in the temperature interval between 40 K and 90 K suggests that electron spin order does not exhibit obvious change in this temperature region. On the other hand, the plasma frequency (or say carrier density) is seen to decrease, but the carrier scattering time is seen to increase from 40 K to 90 K. Therefore, the decrease in conductivity from 40 K to 90 K is not derived from spin disorder, but due to the decrease of the electron's density with temperature in the film. In addition, the film magnetization decreases slowly with temperature from 90 K to 200 K as shown in Fig. 2(b), which indicates the electrons spin tending to lose order slowly. The carrier density as a function of temperature shows a non-monotonous change (Fig. 5(a)), and the carrier scattering time shows a monotonous change (decrease) with temperature (Fig. 5(b)). The decrease in scattering time with temperature is mainly due to the temperature induced electrons spin disorder from 90 K to 200 K. Above 200 K, the LCMO film magnetization decreases rapidly with temperature, which is indicative of the phase transition occurring from FM to PM.

While the carrier scattering time remains at very small value at this high temperature region. Finally, as shown in Fig. 5(c), the fitting Lorentz resonant frequency is seen to increase with temperature from 210 K to 270 K, and the decrease with temperature from 270 K to 290 K. In the temperature range from 210 K to 270 K, the magnetic phase transition occurs as shown in Fig. 2(b) and (d), it is noted that the magnetic phase transition is accompanied with the metal-insulator phase transition, and both kinds of phase transitions take place in the same temperature range from 210 K to 270 K. On the other hand, metal-to-insulator phase transition means Drude-like carriers in metallic phase could be trapped by lattice to form polarons with Lorentz-like conductivity. The strong coupling between spin and polaron leads to the magnetic phase transition taking place at the same temperature as that of metal-to-insulator phase transition [36].

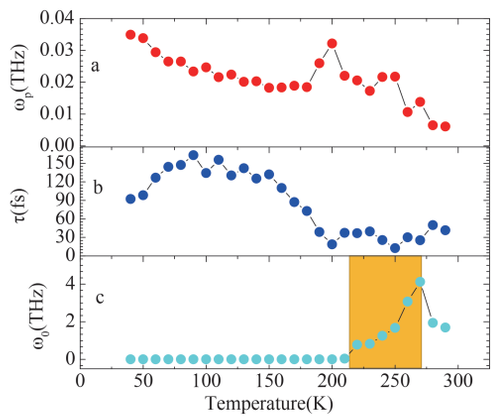

Fig. 5 The temperature dependence of plasma frequency (ω_p) (a), electrons scattering time (τ) (b), and Lorentz resonance frequency (ω_0) (c) of the $La_{0.7}Ca_{0.3}MnO_3$ film in the temperature range from 40 K to 290 K

图5 La0.7Ca0.3MnO3薄膜在40~290 K温度范围内等离子体频率(ωp)(a)、电子散射时间(τ)(b)和洛伦兹共振频率(ω0)(c)与温度的关系

3 Conclusions

In summary, we have investigated the temperature-dependent carrier dynamic of a colossal magnetoresistance LCMO film by terahertz transient spectroscopy. The FM-to-PM phase transition temperature T_C is almost same with the metal-to-insulator phase transition temperature, i.e., T_{MI}=T_C≈260 K. Thus, the FM and PM states are closely related with the metallic and insulating states around T_C≈260 K. At FM phase, the electron spin disorder induces the decrease of the carrier scattering time via weakening the double change energy of the film (90~200 K). Near the phase transition temperature between FM and PM, the rapid decrease of spin order could lead to the decrease in the double exchange energy and density of free carriers in the film. The rapid decrease in double exchange energy leads to the coupling between spin and polaron in the temperature region from 210 K to 270 K. Our work could pave the way to clarify the thermal dynamics of double exchange electrons in $La_{0.7}Ca_{0.3}MnO_3$ film around the Curie temperature T_C. It also improves the analysis of the microscopic mechanism and theory of the film and affords a crucial reference for manganese oxide to be more widely utilized in thermoelectric device, contactless reluctance switch and other devices.

Acknowledgment

This work was supported by National Natural Science Foundation of China (grant numbers 11674213, 61735010, 11647023, 61625505), Natural Science Foundation of Shanghai (grant number 17ZR1411500).

The authors were also grateful to Professors P. K. Siwach and Z. X. Cheng for providing high quality sample.

References

[1] Hong S S, Gu M Q, Manish V, *et al*. Extreme tensile strain states in $La_{0.7}Ca_{0.3}MnO_3$ membranes [J]. *Science*, 2020, **368**(6486): 71-76.
[2] Şen C, Dagotto E. Properties of $La_{0.7}Ca_{0.3}MnO_3$ under extreme tensile strain [J]. *Physical Review B*, 2020, **102**: 035126.
[3] Jin S, Tiefel T H, Mccormack M, *et al*. Thousandfold change in resistivity in magnetoresistive La-Ca-Mn-O films [J]. *Science*, 1994, **264**(5157): 413-415.
[4] Fedorova A V, Chezhina N V. Exchange interactions between atoms of rare-earth elements in the perovskite structure [J]. *Russian Journal of General Chemistry*, 2019, **89**(6): 1136-1141.
[5] Hu M Z, Li S B, Wang C B. Epitaxial growth and multiferroic properties of artificial LCMO/BCZT heterostructure on (100) MgO substrate by pulsed laser deposition [J]. *Journal of Physics D Applied Physics*, 2020, **53**(1): 015002.
[6] Xie Q Y, Zhou X R, Qi C, *et al*. Comparative study of magneto-transport and lattice-vibrational properties of $La_{2/3}Ca_{1/3}MnO_3$ thin films grown on $SrTiO_3$ and $LaAlO_3$ substrates [J]. *International Journal of Modern Physics B*, 2018, **32**(26): 1850287.
[7] Hjelmeland T B, Bazioti C, Gunnæs A E, *et al*. Effect of colossal magnetoresistance material $La_{0.67}Ca_{0.33}MnO_3$ on superconducting properties of $YBa_2Cu_3O_{7-\delta}$ thin films [J]. *Journal of Magnetism and Magnetic Materials*, 2019, **487**: 165335.
[8] Teitelbaum S W, Ofori-Okai B K, Cheng Y H, *et al*. Dynamics of a persistent insulator-to-metal transition in strained manganite films [J]. *Physical Review Letters*, 2019, **123**: 267201.
[9] Gray B A, Middey S, Conti G, *et al*. Superconductor to Mott insulator transition in $YBa_2Cu_3O_7$/$LaCaMnO_3$ heterostructures [J]. *Scientific Reports*, 2016, **6**: 33184.
[10] Lan D, Chen B B, Qu L L, *et al*. Tuning antiferromagnetic interlayer exchange coupling in $La_{0.67}Ca_{0.33}MnO_3$-based synthetic antiferromagnets [J]. *APL Materials*, 2019, **7**(3): 031119.
[11] Li S B, Wang C B, Shen Q, *et al*. Substrate-induced strain effect on magnetic and electrical transport properties of $La_{0.67}Ca_{0.33}MnO_3$ thin films with varying orientation [J]. *Vacuum*, 2019, **164**: 312-318.
[12] Skini R, Khlifi M, Dhahri E, *et al*. Magnetocaloric-transport properties correlation in $La_{0.8}Ca_{0.2}MnO_3$-doped manganites [J]. *Journal of Superconductivity and Novel Magnetism*, 2017, **30**: 3091-3095.
[13] Zener C. Interaction between the d-Shells in the transition metals. II. ferromagnetic ccompounds of manganese with perovskite structure [J]. *Physical Review*, 1951, **82**(3): 403-405.
[14] Culo M, Basletic M, Tafra E, *et al*. Magnetotransport properties of $La_{1-x}Ca_xMnO_3$ ($0.52 \leqslant x \leqslant 0.75$): Signature of phase coexistence [J]. *Thin Solid Films*, 2017, **631**: 205-212.
[15] Mishina E, Sherstyuk N, Sigov A, *et al*. Nonlinear-optical properties of thin $La_{0.7}Ca_{0.3}MnO_3$ films and dynamics of photoinduced phase transition [J]. *Transactions of the Magnetics Society of Japan*, 2004, **4**(4-2): 272-277.
[16] Shatnawi M, Bozin E S, Mitchell J F, *et al*. Nonpercolative nature of the metal-insulator transition and persistence of local Jahn-Teller distortions in the rhombohedral regime of $La_{1-x}Ca_xMnO_3$ [J]. *Physical Review B*, 2016, **93**(16): 165138.
[17] Pantoja A E, Trodahl H J, Buckley R G, *et al*. Raman spectroscopy of orthorhombic $La_{1-x}Ca_xMnO_3$, x = 0.1-0.3 [J]. *Journal of Physics Condensed Matter*, 2001, **13**(16): 3741-3752.
[18] Tank T M, Bodhaye A, Mukovskii Y M, *et al*. Electrical-transport, magnetoresistance and magnetic properties of $La_{1-x}Ca_xMnO_3$ (x=0.12 and 0.3) single crystals [J]. *Journal of Metastable and Nanocrystalline*, 2016, **28**: 65-70.
[19] Liu J W, Wang J J, Gao H T. Infrared emissivities and microwave absorption properties of perovskite $La_{1-x}Ca_xMnO_3$ ($0 \leqslant x \leqslant 0.5$) [J]. *Materials Science Forum*, 2018, **914**: 96-101.
[20] Xia W R, Li L, Wu H, *et al*. Molten salt route of $La_{1-x}Ca_xMnO_3$ nanoparticles: Microstructural characterization, magnetic and electrical transport properties [J]. *Materials Characterization*, 2017, **131**: 128-134.
[21] Mahendiran R, Mahesh R, Raychaudhuri A K, *et al*. Composition dependence of giant magnetoresistance in $La_{1-x}Ca_xMnO_3$ ($0.1 \leqslant x \leqslant 0.9$) [J]. *Solid State Communications*, 1995, **94**(7): 515-518.
[22] Dörr K, De Teresa J M, Müller K-H, *et al*. Preparation and properties of epitaxial $La_{0.7}Ca_{0.3}MnO_{3-\delta}$ films with reduced carrier density [J]. *Journal of Physics Condensed Matter*, 2000, **12**(31): 7099-7109.
[23] Salvato M, Vecchione A, De Santis A, *et al*. Metal-insulator transition temperature enhancement in $La_{0.7}Ca_{0.3}MnO_3$ thin films [J]. *Journal of Applied Physics*, 2005, **97**(10): 103712.
[24] Siwach P K, Singh H K, Srivastava O N. Influence of strain relaxation on magnetotransport properties of epitaxial $La_{0.7}Ca_{0.3}MnO_3$ films [J]. *Journal of Physics Condensed Matter*, 2006, **18**(43): 9783-9794.
[25] Jin S Q, Tiefel T H, Mccormack M, *et al*. Thickness dependence of magnetoresistance in La - Ca - Mn - O epitaxial films [J]. *Applied Physics Letters*, 1995, **67**(4): 557-559.
[26] Arunachalam M, Thamilmaran P, Sakthipandi K. Tunning of metal-insulator phase transition temperature in $La_{0.3}Ca_{0.7}MnO_3$ perovskite material [J]. *Materials Letters*, 2018, **218**: 270-273.
[27] Dong T, Viet V, Shon W H, *et al*. Growth, domain structure, and magnetic properties of $CaMnO_3$ (110) and $La_{0.7}Ca_{0.3}MnO_3$ (110) layers synthesized on the hexagonal $YMnO_3$ (0001) [J]. *CrystEngComm*, 2017, **19**(35): 5269-5274.
[28] Marín L, Gómez M E, Reyes D F, *et al*. Magnetic field dependence of Griffith phase and critical behavior in $La_{0.8}Ca_{0.2}MnO_3$ nanoparticles [J]. *Journal of Magnetism and Magnetic Materials*, 2019, **475**: 374-381.
[29] Hu L Q, Yu L Q, Xiong P, *et al*. Static and dynamic signatures of anisotropic electronic phase separation in $La_{2/3}Ca_{1/3}MnO_3$ thin films under anisotropic strain [J]. *Physics Review B*, 2018, **97**(21): 214428.
[30] Gommert E, Cerva H, Wecker J, *et al*. Influence of misfit stress on the magnetoresistive properties of $La_{0.7}Ca_{0.3}MnO_{3-\delta}$ thin films [J]. *Journal of Applied Physics*, 1999, **85**(8): 5417-5419.
[31] Kida N, Hangyo M, Tonouchi M. Low-energy charge dynamics in $La_{0.7}Ca_{0.3}MnO_3$: THz time-domain spectroscopic studies [J]. *Physical Review B*, 2000, **62**(18): R11965.
[32] Kida N, Hangyo M, Tonouchi M. Low-energy charge dynamics of $La_{0.7}Ca_{0.3}MnO_3$ thin films [J]. *Journal of Magnetism and Magnetic Materials*, 2001, **226**: 818-820.
[33] Ma G H, Li D, Ma H, *et al*. Carrier concentration dependence of terahertz transmission on conducting ZnO films [J]. *Applied Physics Letters*, 2008, **93**(21): 211101.
[34] Jnawal G, Rao Y, Yan H G, *et al*. Observation of a transient decrease in terahertz conductivity of single-layer graphene induced by ultrafast optical excitation [J]. *Nano Letters*, 2013, **13**(2): 524-530.
[35] Lloyd-Hughes J, Jeon T-I. A Review of the terahertz conductivity of bulk and nano-materials [J]. *Journal of Infrared*, Millimeter, and Terahertz Waves, 2012, **33**(9): 871-925.
[36] Hennion M, Moussa F, Rodríguez-Carvajal J, *et al*. Coherent waves of magnetic polarons propagating in $La_{1-x}Ca_xMnO_3$: An inelastic-neutron-scattering study [J]. *Physical Review B*, 1997, **56**(2): R497-R500.